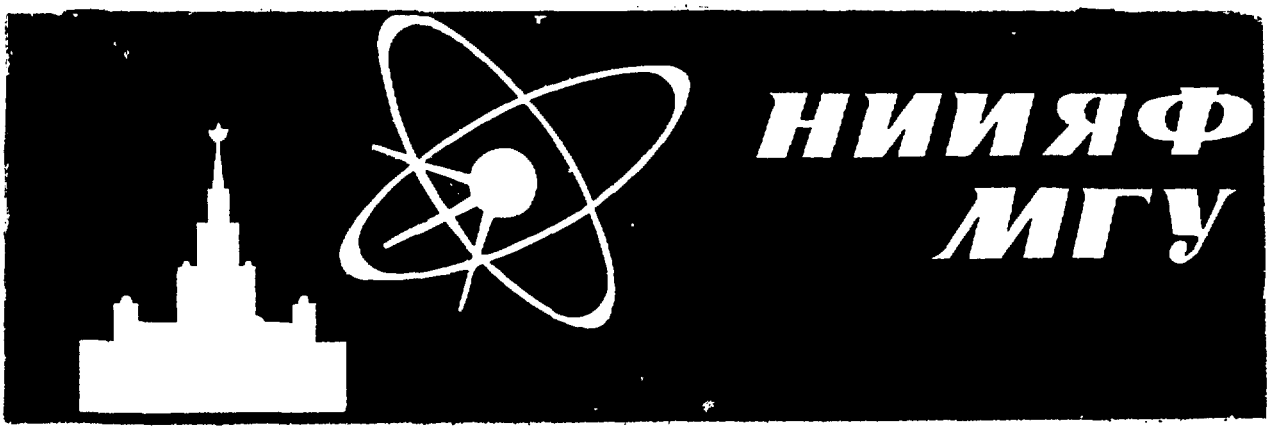

Preprint - 90 - 42/188.

INP-MSU--90-42-188

A.M.Anokhina, V.I.Galkin,

I.P.Ivanenko, T.M.Roganova

METHOD OF SEPARATION OF AIR SHOWERS INITIATED BY γ-QUANTA AND PROTONS USING CERENKOV LIGHT ANGULAR CHARACTERISTICS IN COMBINATION AND ANGULAR RESOLUTION ESTIMATE FOR AN ARRAY OF SEVERAL OPTICAL TELESCOPES

MOSCOW 1990

NUCLEAR PHYSICS RESEARCH INSTITUTE

MOSCOW STATE UNIVERSITY

Preprint - 90 - 42/188.

A.M.Anokhina, V.I.Galkin,

I.P.Ivanenko, T.M.Roganova

METHOD OF SEPARATION OF AIR SHOWERS INITIATED BY γ-QUANTA AND PROTONS USING CERENKOV LIGHT ANGULAR CHARACTERISTICS IN COMBINATION AND ANGULAR RESOLUTION ESTIMATE FOR AN ARRAY OF SEVERAL OPTICAL TELESCOPES

MOSCOW 1990

ABSTRACT

Computer simulation of optical characteristics of air showers was carried out. On the basis of multidimensional analysis of Cerenkov light angular distribution possibility is considered to distinguish γ-showers from proton showers. Also an estimate for angular resolution is given for an array of five optical telescopes situated at Mt.Aragats.

Authors:

Anokhina A.M., Galkin V.I., Ivanenko I.P., Roganova T.M.

... there is still a reality left there to love, when the illusions have vanished.

COLIN WILSON
"The Mind Parasites"

INTRODUCTION.

Modern stage of high-energy cosmic γ-ray emission research is characterized by heightened needs for the reliability of identification of the so-called "γ-events", i.e. γ-initiated showers.

One can obtain information of primary γ-quanta of energy $\geq$ 1 TeV by detecting secondaries born in interactions of gammas with Earth atmosphere. In this case the task of an experiment reduces to reliable selection of γ-initiated electron-photon cascades against the background of air showers caused by primary nuclei. The main problem is that with angular resolution of experimental array of the order of $\sim 1^{\circ}$ primary cosmic ray flux makes $\sim 5 \cdot 10^{-9}$ cm$^{-2} \cdot$ s^{-1} which by far exceeds estimated γ-quantum flux $\sim 10^{-11} - 10^{-12}$ cm$^{-2} \cdot$ s^{-1} ($E_{\gamma} \geq 1$ TeV) [1].

In the energy band $E_{\gamma} \leq 10^{12}$eV optical systems are used for search and detection of γ-showers -- special telescopes aimed at Cerenkov emission of charged shower particles. Lower limit for energy of γ-ray detected in such a way is $\sim 10^{11}$eV, which is due to minimum Cerenkov photon density required, detector threshold sensitivity, light-collecting area and night sky background.

As far as primary nuclei background suppression is concerned, angular distribution of Cerenkov light generated by γ- and p-showers is worth paying special attention to. Differences in Cerenkov light angular distribution effect shower images one can obtain in focal plane of a mirror of a Cerenkov telescope and, therefore, analyzing such images one can get information on the types of primary particles that initiated the corresponding showers.

In order to construct selection criterion and evaluate its efficiency various characteristics of images (Cerenkov light spots) are used. Note that experimental investigation is possible only for background events (i.e. proton showers). In case of γ-showers the only way to obtain Cerenkov image characteristics is to carry out a calculation (most likely, numerical or Monte-Carlo). Each specific experimental array requires a calculation of its own, because the results of such calculations are very sensitive to the conditions of particular experiment (e.g. observation height, geometry of light receiver, mirror area, etc.).

Simulations of Cerenkov angular images of showers in Whipple observatory telescope carried out by Hillas [2] show that there exist some Cerenkov light spot characteristics that really can help us to identify the primary particle type. They are: the so-called azimuthal width A (the way Hillas put it)

$$A = \sqrt{L^2 \cdot \sin^2\omega + W^2 \cdot \cos^2\omega} \ ,$$

where L - spot length, W - spot width, ω - angle between the spot long axis and "center of spot - center of detector" direction, and MISS - the distance between the center of detector and the spot long axis.

Using MISS distribution for γ-showers Hillas [3] estimates the accuracy of γ-source direction determination with the help of two telescopes (stereovision) to be ~ few angular minutes.

In present paper characteristics of Cerenkov spots are investigated on the basis of simulation of optical emission from electron-photon and proton showers of $E_o = 10^{12}, 10^{13}, 10^{14}$ eV and γ-shower selection criterion is constructed; algorithm is developed enabling γ-source direction determination to within $\leq 0^{\circ}.2$ using several telescopes.

While calculating angular characteristics of proton and electron-photon cascade optical emission a method is used similar to the one described in [4].

Simulations are carried out for an array of five telescopes set 70 m apart at observation depth 700 g/cm^2.

I. IMAGES IN A SINGLE TELESCOPE: PROCESSING & CLASSIFICATION.

§ 1. LIGHT SPOT PROCESSING DESCRIPTION.

Cerenkov light images were obtained as the result of simulation of optical emission angular distribution in a detector consisting of a spherical mirror of area 5 m^2 and a matrix of 100 angular cells -- light receivers which were situated in focal plane of the mirror. Each cell views a solid angle of $0.^{\circ}3 \times 0.^{\circ}3$, the whole matrix enveloping $3^{\circ} \times 3^{\circ}$.

Light spot in such a detector is a two-dimensional distribution of Cerenkov light over 100 angular cells.

Spot handling procedure was as follows:

1. Maximal-light-deposit cell coordinates & contents are found as well as signal totaled over the whole matrix (Q).
2. Coordinates of the spot center of mass are determined:

$$\bar{X} = \frac{\sum_{i=1}^{n} X_i \cdot W_i}{\sum_{i=1}^{n} W_i}, \qquad \bar{Y} = \frac{\sum_{i=1}^{n} Y_i \cdot W_i}{\sum_{i=1}^{n} W_i},$$

where X_i, Y_i - coordinates of i-th cell center, W_i - its light contents, $n \leq 100$. Only cells with contents exceeding 1% of Q are taken into account.

3. Distance RM between the spot center of mass and the center of the detector field of view is defined.
4. Spot second momenta are determined including the centered ones:

$$\bar{X^2} = \frac{\sum_{i=1}^{n} X_i^2 \cdot W_i}{\sum_{i=1}^{n} W_i}; \qquad \bar{Y^2} = \frac{\sum_{i=1}^{n} Y_i^2 \cdot W_i}{\sum_{i=1}^{n} W_i};$$

$$\overline{XY} = \frac{\sum_{i=1}^{n} (X_i - \bar{X}) \cdot (Y_i - \bar{Y}) \cdot W_i}{\sum_{i=1}^{n} W_i} ;$$

$$D_X = \frac{\sum_{i=1}^{n} (X_i - \bar{X})^2 \cdot W_i}{\sum_{i=1}^{n} W_i} ; \qquad D_Y = \frac{\sum_{i=1}^{n} (Y_i - \bar{Y})^2 \cdot W_i}{\sum_{i=1}^{n} W_i} .$$

5. The lengths of the spot long (SA) and short (SB) axes are calculated, orientation of spot in regard to detector frame is determined. On this occasion the spot is approximated by two-dimensional normal law:

$$P(X,Y) = \frac{1}{\sqrt{(2\pi)^2 \cdot \det \lambda_{ij}}} \cdot \exp\left\{ -\frac{1}{2} \sum_{j=1}^{2} \sum_{k=1}^{2} A_{jk}(X-\bar{X})(Y-\bar{Y}) \right\} ;$$

where λ_{jk} is the covariance matrix: $\lambda_{jk} = \begin{bmatrix} \sigma_X^2 & r\sigma_X\sigma_Y \\ r\sigma_X\sigma_Y & \sigma_Y^2 \end{bmatrix}$;

$A_{jk} = \lambda_{jk}^{-1}$; $\sigma_X = \sqrt{D_X}$; $\sigma_Y = \sqrt{D_Y}$; $r = \overline{XY} / (\sigma_X\sigma_Y)$.

In order to calculate SA and SB the distribution is diagonalized which gives:

$$SA^2 = \sigma_1^2 = \frac{1}{2M} , \qquad SB^2 = \sigma_2^2 = \frac{1}{2L} , \quad \text{where}$$

$$M = \frac{1}{4(1-r^2)\sigma_X^2\sigma_Y^2} \cdot \left[\sigma_X^2 + \sigma_Y^2 - \frac{(\sigma_X^2 - \sigma_Y^2)^2 - 4r^2\sigma_X^2\sigma_Y^2}{\sqrt{(\sigma_X^2 - \sigma_Y^2) + 4r^2\sigma_X^2\sigma_Y^2}} \right] ,$$

$$L = \frac{1}{4(1-r^2)\sigma_X^2\sigma_Y^2} \cdot \left[\sigma_X^2 + \sigma_Y^2 + \frac{(\sigma_X^2 - \sigma_Y^2)^2 - 4r^2\sigma_X^2\sigma_Y^2}{\sqrt{(\sigma_X^2 - \sigma_Y^2) + 4r^2\sigma_X^2\sigma_Y^2}} \right] .$$

6. Angle ω between the spot long axis and "spot center of mass - center of detector" direction is calculated (see Fig.1).

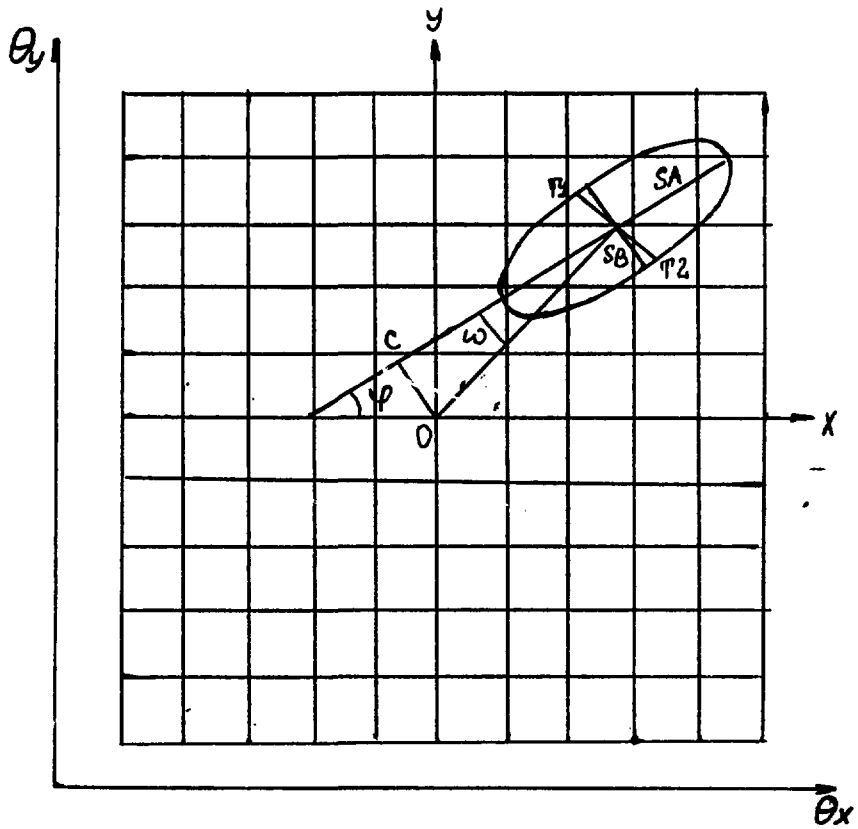

Fig. 1

Scheme explaining the process of shower light image handling.
SA and SB - long and short spot axes (more exactly, semi-axes),
[T1,T2] segment - spot azimuthal width (AZWID),
φ - spot long axis orientation angle,
ω - angle between the spot long axis and "spot center of mass - center of detector" direction,
[O,C] segment - distance between the center of detector and the spot long axis (HMISS).

7. Azimuthal width AZWID is calculated, i.e. [T1,T2] segment (see Fig.1):

$$AZWID = \frac{2 \cdot a \cdot b}{\sqrt{a^2 \cdot \cos^2\omega + b^2 \cdot \sin^2\omega}}, \quad a = SA, \quad b = SB.$$

8. Distance between the center of detector and the spot long axis, i.e. [O,C] segment length is calculated:
HMISS = RM · sin ω .

9. Value is calculated of SUPER parameter incorporating several light spot characteristics:

$SUPER = \frac{SB}{SA} \cdot |\omega| \cdot RM$. Such parameter form is chosen according to considerations based on [2,3] data and our results that each factor of a composite parameter should be smaller (or greater) for γ-showers than for proton ones. In the case under consideration, γ-shower light images are:

1) more stretched: $\left[\frac{SB}{SA}\right]_\gamma < \left[\frac{SB}{SA}\right]_p$,

2) oriented mainly towards the center of detector:

$\omega_\gamma < \omega_p$,

3) closer to the center of detector: $RM_\gamma < RM_p$.

§ 2. Γ/P-SELECTION CRITERION CONSTRUCTION PROCESS.

After individual image processing is completed the event (i.e. this particular image) can be represented by N-dimensional random vector X the way it was done in [4]. Then a question is investigated which of the two classes $(\omega_\gamma, \omega_p)$ X belongs to. Distribution of each component of vector X is approximated by normal one. Each class of events $(\omega_i, i=1,2)$ is characterized by mean vector ξ_i and covariance matrix λ^i that define normal conditional probability density function:

$$P(X/\omega_i) = \frac{1}{\sqrt{(2\pi)^N \cdot |\lambda^i|}} \cdot \exp\left\{ -\frac{1}{2} \sum_{j=1}^{N} \sum_{k=1}^{N} A^i_{jk} (X_j - \xi_k)(X_k - \xi_k) \right\}$$

where ξ^i_k - k-th component of mean vector ξ^i corresponding to

class i, matrix $A^i = [\lambda^i]^{-1}$.

Mean vectors and covariance matrices are calculated using the whole population of each of the two classes (p,γ), then each particular event's native class is determined.

Shower-type-recognizing criterion is based on Bayes rule minimizing the probability of erroneous decision [5]:

$$CR = \frac{P(\omega_p)\cdot P(X/\omega_p)}{P(\omega_\gamma)\cdot P(X/\omega_\gamma)} \gtrless 1 \Rightarrow \begin{cases} \omega_p \\ \omega_\gamma \end{cases} \qquad (*)$$

where $P(\omega_p)$ and $P(\omega_\gamma)$ - a priori probabilities of the corresponding classes of events.

§ 3. RESULTS OF ANGULAR IMAGE PROCESSING AND CLASSIFICATION.

As a result of simulation γ and proton shower database was created for primary energies 10^{12}, 10^{13}, 10^{14}eV. Sample sizes for each evert class are presented in Table 1.

Table 1

Energy, eV	10^{12}	10^{13}	10^{14}
γ-showers	100	100	100
p-showers	300	300	300

Shower axes were uniformly spreaded around detector within a circle of radius 100 m with center coinciding with the detector center. Furthermore, proton shower directions were uniformly spreaded within a vertical cone of 2 x 1°5 top angle.

While calculating shower light images night sky background was taken into account. Mean stellar light flux gathered by 5 m^2-mirror was calculated, then individual background photon number for each light receiver was sampled from Poisson distribution.

To estimate the effect of PMT current fluctuations, Cerenkov images were simulated both taking these fluctuations into

account and neglecting them. They influenced light image characteristics and classification results mostly at $E=10^{12}$eV.

Figures 2-6 show light image mean characteristics for γ and p-showers of the three primary energies. Table 2 contains mean values (M) and dispersions (D). Using these plots and Table 2, one can conclude that:

1. Mean values of SA, SB, AZWID, i.e. of the light image size parameters, decrease with increasing primary energy. Proton shower images are larger than γ-shower ones, but the differences decrease as primary energy grows. Switching on PMT current fluctuations enlarges γ and p-shower light images.

2. PMT fluctuations effect image size parameter dispersions in a more complicated way. At $E_o = 10^{12}$eV they increase SA, SB, AZWID dispersions of γ-shower images and decrease similar values of p-shower images (the latter is due to low photon density and large image size of p-showers and discrete structure of telescope). As primary energy grows ($E_o = 10^{13}$and 10^{14}eV) SA, SB, AZWID dispersions diminish.

3. Light image compound parameters SUPER and HMISS display different behaviour for γ and p-showers with primary energy. SUPER mean value increases steeply for p-showers and drops abruptly for γ-showers as E_o varies from 10^{12}eV to 10^{13}eV. 10^{13}eV - 10^{14}eV transition changes SUPER relatively smoothly. HMISS shows similar behaviour. Dispersions of these parameters decrease (increase) slowly with E_o for γ-(p-)showers.

Comparing Fig. 2, 3, 4 to Fig. 5, 6 one can realize that differences in spot sizes are the most pronounced at $E_o = 10^{12}$eV and almost vanish at $E_o = 10^{14}$eV while SUPER and HMISS mean values remain different for γ and p-showers.

Classification was carried out using five parameters SA, SB, AZWID, SUPER, HMISS which gave the best results in combination. Correlation coefficients of these parameters for various primary energies are presented in Tables 3-6.

As one can see from the tables, compound parameters SUPER and HMISS correlate weakly with other parameters which does much good to the selection criterion. AZWID correlations

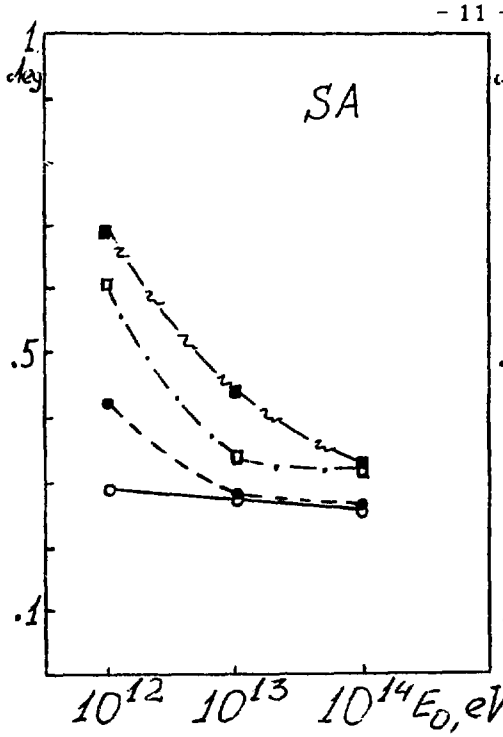

Fig. 2

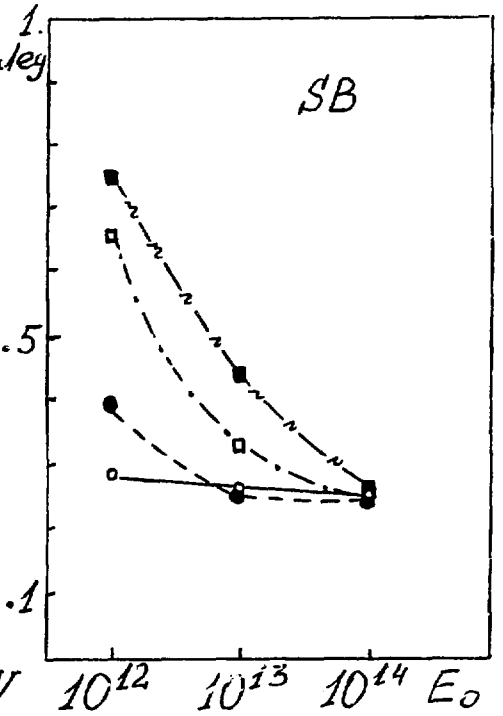

Fig. 3

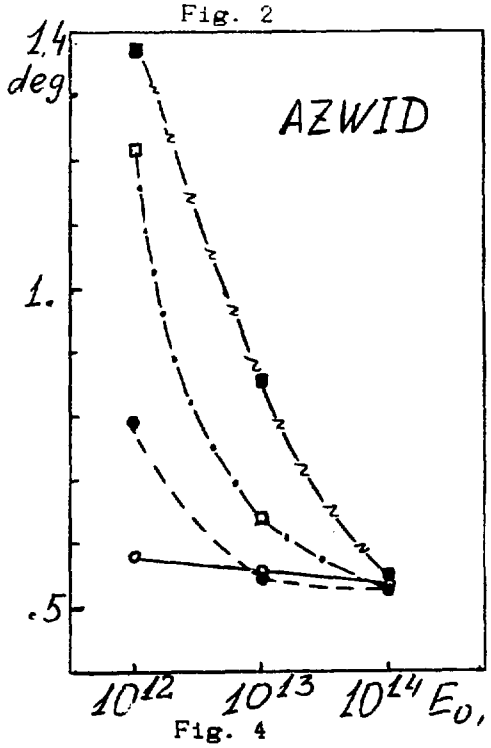

Fig. 4

Light image size parameter dependences on primary energy

o----- γ, without PMT current fluctuations;

●- - - γ, PMT current fluctuations taken into account;

□-·-·- p, without PMT current fluctuations;

■--∞-- p, PMT current fluctuations taken into account.

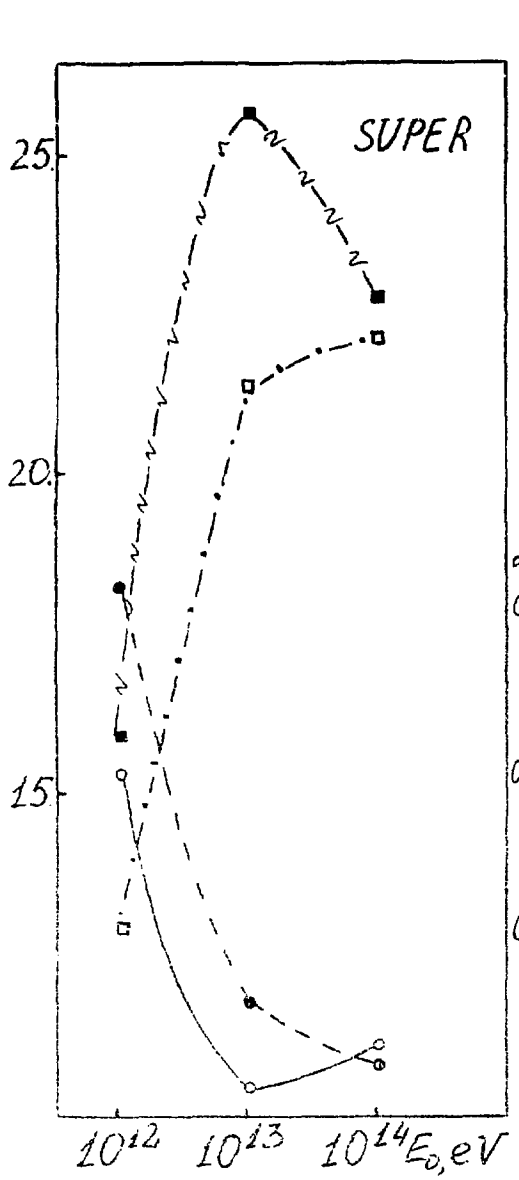

o----- γ, without PMT current fluctuations;

●- - - γ, PMT current fluctuations taken into account;

□-·-·- p, without PMT current fluctuations;

■--∞-- p, PMT current fluctuations taken into account.

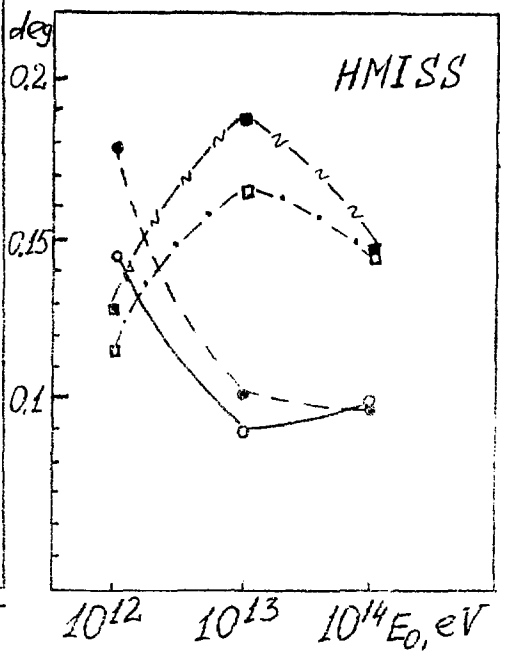

Fig. 5

Fig. 6

Light image compound parameter dependences on primary energy

Table 2

Sample mean values (M) and dispersions (D) of light image parameters

E_o, eV \ image par		SA		SB		AZWID		SUPER		HMISS	
		γ	p	γ	p	γ	p	γ	p	γ	p
10^{12}, PMT fluc. off	M	.29	.61	.29	.67	.58	1.23	15.3	15.9	.14	.12
	D	.002	.045	.002	.071	.006	.213	161.	211.	.084	.087
10^{12}, PMT fluc. on	M	.42	.69	.39	.75	.79	1.42	18.2	12.9	.18	.13
	D	.017	.024	.018	.028	.069	.083	171.	108.	.123	.036
10^{13}, PMT fluc. off	M	.27	.33	.28	.33	.55	.65	10.4	25.7	.09	.16
	D	.002	.016	.002	.033	.006	.079	106.	475.	.051	.272
10^{13}, PMT fluc. on	M	.27	.44	.28	.44	.55	.86	11.8	21.3	.10	.19
	D	.002	.033	.002	.043	.006	.125	124.	266.	.059	.152
10^{14}, PMT fluc. off	M	.26	.32	.27	.26	.53	.53	11.1	22.7	.10	.14
	D	.002	.010	.002	.009	.008	.027	80.1	350.	.045	.366
10^{14}, PMT fluc. on	M	.26	.32	.27	.26	.54	.55	10.8	22.1	.10	.14
	D	.002	.010	.002	.011	.009	.033	87.9	239.	.043	.392

with SA and SB reflect real spot geometry (see Fig. 1).

Classification results for individual γ and p-shower images of various primary energies using the five parameters mentioned above (SA, SB, AZWID, SUPER, HMISS) and neglecting PMT current fluctuations are presented in Table 7. Similar results including PMT current fluctuations according to Poisson distribution are given in Table 8.

Table 3

Correlation coefficients ($E_o = 10^{12}$eV, PMT fluctuations off)

		SB	AZWID	SUPER	HMISS
SA	gamma	-0.39	-0.35	-0.01	0.08
	proton	0.60	0.77	0.51	0.23
SB	gamma		0.99	0.03	-0.26
	proton		0.89	-0.14	-0.28
AZWID	gamma			-0.01	-0.21
	proton			-0.37	-0.26
SUPER	gamma				0.34
	proton				0.36

Table 4

Correlation coefficients ($E_o = 10^{12}$eV, PMT fluctuations on)

		SB	AZWID	SUPER	HMISS
SA	gamma	0.57	0.64	-0.12	0.03
	proton	0.19	0.39	-0.36	-0.02
SB	gamma		0.99	-0.08	-0.05
	proton		0.85	0.09	-0.14
AZWID	gamma			-0.07	-0.03
	proton			-0.17	-0.03
SUPER	gamma				0.28
	proton				0.50

One can see from Tables 7 and 8 that PMT current fluctuations effect classification most at $E_o = 10^{12}$eV and are negligible at $E_o = 10^{14}$eV.

Classification was carried out with the help of a parameter called CRITER (CRITER = ln CR , see (*)) , which value was calculated for each γ and p-event. Classification results presented in Table 8 were obtained using 0.0 as a criterion border, i.e. if CRITER value was greater than 0.0 the event was

Table 5

Correlation coefficients ($E_o = 10^{13}$eV, PMT fluctuations on)

		SB	AZWID	SUPER	HMISS
SA	gamma	-0.07	-0.04	0.06	0.21
	proton	0.49	0.63	-0.33	-0.07
SB	gamma		0.99	0.18	-0.09
	proton		0.93	-0.01	-0.02
AZWID	gamma			0.15	-0.04
	proton			-0.09	-0.02
SUPER	gamma				0.28
	proton				0.37

Table 6

Correlation coefficients ($E_o = 10^{14}$eV, PMT fluctuations on)

		SB	AZWID	SUPER	HMISS
SA	gamma	0.15	0.17	-0.04	-0.01
	proton	-0.19	-0.05	-0.24	-0.02
SB	gamma		0.99	0.13	-0.003
	proton		0.96	-0.09	-0.02
AZWID	gamma			0.08	-0.03
	proton			-0.07	-0.02
SUPER	gamma				0.47
	proton				0.17

treated as "proton"-type, otherwise it was called "gamma"-event. One can improve classification of images including PMT current fluctuations by shifting the criterion border. For instance, 100% of proton events at $E_o = 10^{13}$eV are identified correctly if value CRITER = -1 is adopted as a border one. In this case 6% of γ-showers are treated as p-showers. At $E_o = 10^{12}$eV 100% of proton showers are recognized as such, if the

Table 7

Classification results (PMT fluctuations off)

Primary part. type / Prim. energy, eV	γ		p	
	identified as γ-showers	identified as p-showers	identified as γ-showers	identified as p-showers
10^{12}	100 (100%)	0 (0%)	0 (0%)	300 (100%)
10^{13}	93 (93%)	7 (7%)	0 (0%)	300 (100%)
10^{14}	94 (94%)	6 (6%)	0 (0%)	100 (100%)

Table 8

Classification results (PMT fluctuations according to Poisson law)

Primary part. type / Prim. energy, eV	γ		p	
	identified as γ-showers	identified as p-showers	identified as γ-showers	identified as p-showers
10^{12}	92 (92%)	8 (8%)	5 (1.7%)	295(98.3%)
10^{13}	95 (95%)	5 (5%)	1 (0.03%)	299(99.7%)
10^{14}	94 (94%)	6 (6%)	0 (0%)	100 (100%)

criterion border is moved to -5. Simultaneously 37% of γ-showers are identified as p-showers.

II. ARRIVAL DIRECTION AND CORE LOCATION RECONSTRUCTION.

§ 1. CORE LOCATION ESTIMATION.

Primary particle arrival direction is assumed to coincide with shower axis. One can define shower axis by locating any two points belonging to it. Images in five telescopes simultaneously viewing a shower are used to define its axis. In order to consider a possibility of primary particle arrival direction determination simulation was carried out of light angular distribution simultaneously in five telescopes, forming a centered square with a side 100 m (see Fig. 7). Such pattern was accepted by ANI project for "Gamma" array (Mt. Aragats).

Fig. 7

To find coordinates of the first of the two points used to determine axis direction, a set of light fluxes Q_i, $i=1,\ldots,5$ detected by five telescopes is analyzed. Assuming shower axis is the axis of symmetry of light lateral distribution one can use Q_i to calculate the coordinates of its center of symmetry at the observation level, which nearly coincides with the point where the shower axis crosses the observation level, if shower zenith angle $\alpha \leq 3^\circ$. To estimate R_i (core distance set for the five detectors) one should compare Q_i to the mean light lateral distribution function of electron-photon shower. The latter is defined as mean light flux Q (within telescope field of view) dependence on core distance R and assumed to look like

$$Q(R) = \frac{Q_o \cdot R}{(1 + R/R_o)^{\alpha}}$$

While fitting lateral distribution in core distance range 20 - 100 m using 100 γ-showers of $E_o = 10^{12}$eV the following

values are obtained:

$Q_o = 7.6 \cdot 10^4$ photon/m^2, $R_o = 46.8$ m, $\alpha = 4.44$.

Sample used for the fit consists of showers uniformly spreaded over 100m-radius circle around the center of telescope array. Rapid fall of the light flux for the given aperture ($1^\circ.5$ half angle) at $R \gtrsim 100$ m for $E_o = 10^{12}$eV (Fig. 8) limits effective detection area to $3 \cdot 10^4$ m^2. One can draw the same conclusion from calculation [6].

By minimizing a functional

$$F = \sum_{i=1}^{5} (1 + Q_i / Q(R_i))$$

(Q_i - total light flux value in i-th telescope) over x,y and Q_o disribution center-of-symmetry coordinates x_o , y_o are found. Point (x_o , y_o , z_{det}) (here z_{det} - observation level height) is accepted as one of the two points defining the shower axis. For 50 vertial showers hitting the ground not farther than 100 m from the central telescope, core-locating procedure precision dependence on core distance ("shower core - central detector" distance) was analyzed. Results are summarized in Table 9.

Table 9

Core distance range, m	Core location precision, m
0 - 30	3.3
30 - 50	7.5
50 - 70	13.9
70 - 100	16.5

Mean core location precision for vertical showers is 10 m , for inclined showers ($\pm 1^\circ.5$) -- 20 m.

Similar procedure defining shower axis intersection with array plane and other shower parameters was used, for example, for balloon EAS experiment [7] data processing (core

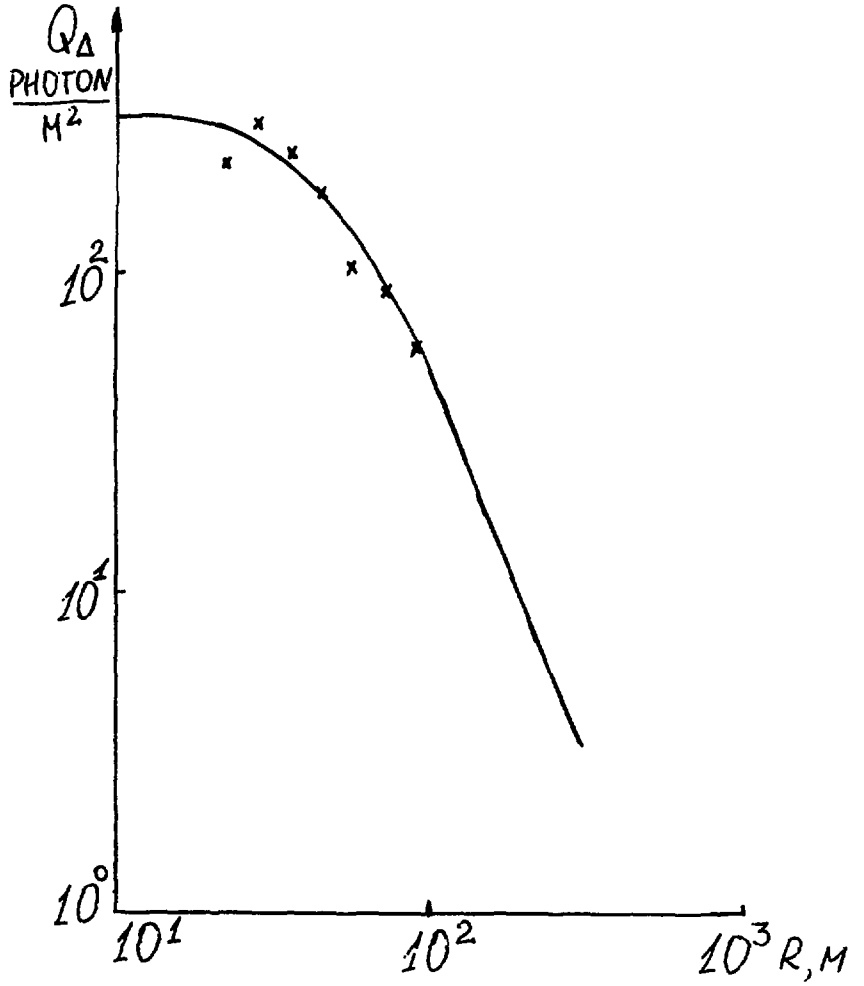

Fig. 8

Photon flux density dependence on core distance R. Telescope reception solid angle $3^\circ \times 3^\circ$. Solid line - approximation.

location precision varied from 1.7 m to 18.4 m with core distance range changing from 0-5 m to 45-50 m).

§ 2. ARRIVAL DIRECTION RECONSTRUCTION USING LIGHT IMAGE CHARACTERISTICS.

Second point coordinates (p.A, Fig. 9) are obtained by iterations using light image "center-of-mass" angular coordinates in each of five telescopes.

Zero-order approximation for p.A coordinates is defined using any two of the five detectors in the following way. Let ϑ_{xc1} , ϑ_{yc1} be light spot center-of-mass coordinates in the first detector, ϑ_{xc2} , ϑ_{yc2} - the same in the second detector. Azimuth ϑ_1 and zenith ψ_1 set the direction D1-T1 toward shower maximum of emission in regard to the first detector. ϑ_2 and ψ_2 set similar direction D2-T2 in regard to the second detector. Generally, straight lines D1-T1 and D2-T2 do not intersect. To fix a point in space, first of all, p.A projection on the observation plane is defined from equations describing projections of lines D1-T1 and D2-T2 on the same plane:

$$\begin{cases} (X - XD1) = (Y - YD1) * \operatorname{tg} \vartheta_1 , \\ (X - XD2) = (Y - YD2) * \operatorname{tg} \vartheta_2 , \end{cases}$$

where (XD1 , YD1) and (XD2 , YD2) are coordinates of the first and the second detectors, respectively. Hence it appears:

$$\begin{cases} X = \dfrac{(XD1 * \operatorname{tg} \vartheta_2 - XD2 * \operatorname{tg} \vartheta_1 + YD2 - YD1)}{\operatorname{tg} \vartheta_1 - \operatorname{tg} \vartheta_2} \\ Y = (X - XD2) * \operatorname{tg} \vartheta_2 + YD2 \end{cases}$$

Then, using (X , Y) and equations for D1-T1 and D2-T2, Z1 and Z2 (see Fig. 9) are calculated:

$$Z1 = \frac{X - XD1}{\cos \vartheta_1} * \operatorname{ctg} \psi_1 , \qquad Z2 = \frac{X - XD2}{\cos \vartheta_2} * \operatorname{ctg} \psi_2 .$$

Coordinate z of p.A estimate is calculated as an average between Z1 and Z2: $z = (Z1 + Z2)/2$.

Similar procedure is applied to each pair of five detectors

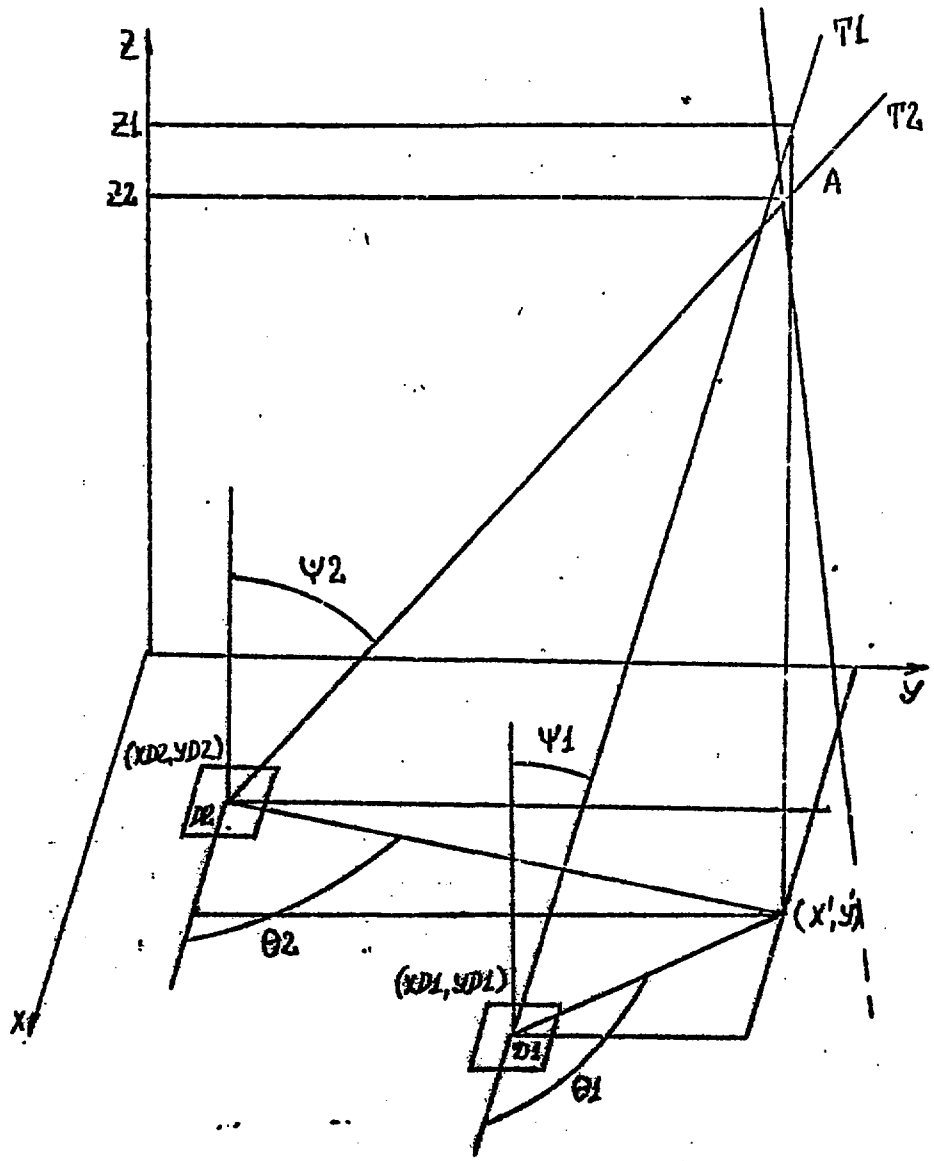

Fig. 9

Scheme illustrating a procedure of building an estimate for p.A (the second point that belongs to the shower axis).

(on the whole 10 pairs), and, finally, average over all ten estimates is used as zero-order approximation.

For 50 vertical and 25 inclined (not more than $1^{\circ}.5$ in regard to the vertical) showers of $E_o = 10^{12}$eV , with axes uniformly spread within a circle of radius 100 m , light images in five telescopes were simulated. For each shower an angle was calculated between the true axis direction (registered during simulation) and the direction defined by core location and p.A estimates. Mean error value for vertical showers was $\bar{\beta}_{vert} = 0^{\circ}.38$ ($\sigma = 0^{\circ}.26$), while the one for inclined showers was $\bar{\beta}_{incl} = 4^{\circ}.23$ ($\sigma = 9^{\circ}.97$).

To make p.A estimate closer to reality, it was taken into consideration that Cerenkov light spot is described by two-dimensional normal distribution with RMS deviations corresponding to spot long (SA) and short (SB) axes lengths. As one can learn from part I of this paper, SA and SB for γ-showers do not exceed $0^{\circ}.3$. It seems natural to assume the precision of Gaussian distribution center estimate to be about $0^{\circ}.3$. However, simultaneous consideration of data of all available telescopes can make p.A estimate substantially more exact, has one assumed that spot centers in all telescopes correspond to one and the same area in three-dimensional space. Such consideration comes to a search for a point in space, which is the best fit to the directions given by five spot centers. In the simplest case, one can look for a point with minimum sum of distances to straight lines D1-T1, D2-T2,... To take spot "center-of-mass" estimate errors in a separate telescope into account, a functional using data of n detectors ($n \leq 5$)

$$F(x,y,z) = \sum_{i=1}^{n} f\left[\vartheta_{xi}(x,y,z) - \vartheta_{xci}\right] + f\left[\vartheta_{yi}(x,y,z) - \vartheta_{yci}\right]$$

is minimized over (x,y,z). Here ϑ_{xci} , ϑ_{yci} - angular

coordinates of spot "center-of-mass" in i-th telescope; ϑ_{xi} , ϑ_{yi} - angular coordinates of emission maximum (p.A) in i-th detector; $f(\vartheta)$ is a weight function:

$$f(\vartheta) = \begin{cases} \vartheta * a + b & , \ \vartheta > 0^{\circ}.15 \text{ or } \vartheta < -0^{\circ}.15 , \\ \exp\left(\frac{\vartheta - d}{c} \right) & , \ 0^{\circ}.0 < \vartheta \leq 0^{\circ}.15 , \\ \exp\left(\frac{d - \vartheta}{c} \right) & , \ -0^{\circ}.15 < \vartheta \leq 0^{\circ}.0 . \end{cases}$$

Weight function shape is plotted in Fig. 10. One can see that small and slowly changing weight corresponds to the central $\pm 0^{\circ}.15$ region, while periphery is provided with rather steep slopes. Calculations show that the precision of axis direction estimation does not depend on weight function wing slope as well as on its magnitude.

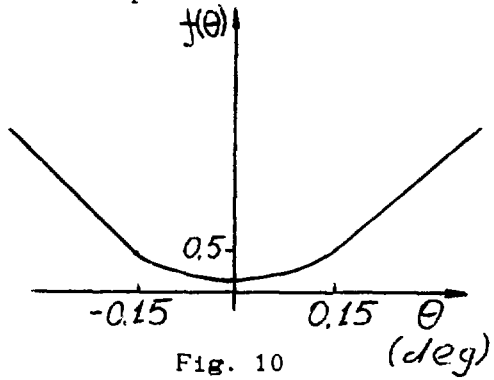

Fig. 10

Using this optimizing procedure improved p.A estimates were obtained for each shower. Corresponding axis direction errors are: $\bar{\beta}_{vert} = 0^{\circ}.34$ ($\sigma = 0^{\circ}.24$) , $\bar{\beta}_{incl} = 0^{\circ}.83$ ($\sigma = 0^{\circ}.66$).

One can improve axis direction estimation precision by taking orientation of light spot in regard to detector frame of reference into account. For example, one can determine p.A using not ϑ_{xci} , ϑ_{yci} but directions given by "upper" edges of spots:

$\vartheta_{xi} = \vartheta_{xci} - SA * \cos\varphi$; $\vartheta_{yi} = \vartheta_{yci} - SA * \sin\varphi$, where SA - spot long axis size, φ - spot long axis orientation angle. Axis direction estimation precision dependence on core distance (measured in regard to the central detector) for 50 vertical showers is given in Table 10. Here all triggered telescopes

take part in direction estimating procedure. Mean direction estimation precision is $\bar{\beta}_{vert} = 0^{\circ}.17$ ($\sigma = 0^{\circ}.13$). Direction estimation precision dependence on the number of triggered detectors is presented in Table 11. Left column shows array configuration.

Table 10

Core distance range, m	Axis direction precision, deg
0 - 30	0.07
30 - 50	0.12
50 - 70	0.17
70 - 100	0.18

Table 11

Array configuration	Axis direction precision, deg
o o o o o	$\bar{\beta} = 0.15$ ($\sigma = 0.12$)
o o o o	$\bar{\beta} = 0.15$ ($\sigma = 0.09$)
o o o	$\bar{\beta} = 0.22$ ($\sigma = 0.12$)
o o	$\bar{\beta} = 0.50$ ($\sigma = 0.28$)

For 25 inclined showers mean direction precision is $\beta_{incl} = 0^{\circ}.67$ ($\sigma = 0^{\circ}.87$).

CONCLUSION.

On the basis of simulation of optical emission of γ- and p-showers of $E_o = 10^{12}$, 10^{13}, 10^{14}eV is shown that multidimensional analysis of shower images in focal plane of telescope mirror gives a possibility to identify correctly all proton-initiated showers with only $\sim$ 10% loss of γ-showers.

An algorithm is developed of shower axis direction estimation and shower core location using shower light images detected simultaneously by several telescopes.

REFERENCES:

1. S.I.Nikolsky : Voprosy atomnoy nauki i tekhniki, Release 2/33/, 1987, p.3-11.

2. A.M.Hillas : Proc. Int. Workshop on VHE Gamma Ray Astronomy, Crimea, USSR, 1989, p.130-133.

3. A.M.Hillas : Proc. Int. Workshop on VHE Gamma Ray Astronomy, Crimea, USSR, 1989, p.134-137.

4. T.A.Chuykova, V.I.Galkin, I.P.Ivanenko, T.M.Roganova : Proc. 20th ICRC, 1987, v.6, p.97-100.

5. S.A.Aivazyan, V.M.Buchstaber, I.S.Yenyukov, L.D.Meshalkin : Applied Statistics (classification and reduction of dimensionality), Moscow, Finansy i statistika, 1989, p.47.

6. R.Browing, K.E.Turver : Nuovo Cimento, 1977, v.38A, p.223.

7. V.A.Kuzmin : Thesis, Moscow State University, Institute of Nuclear Physics, 1985.

Анна Михайловна Анохина

Владимир Игоревич Галкин

Игорь Павлович Иваненко

Татьяна Михайловна Роганова

Методика разделения атмосферных ливней от γ-квантов и протонов по совокупности угловых характеристик черенковского излучения и оценка углового разрешения системы из нескольких оптических телескопов

Препринт НИИЯФ МГУ - 90- 42/188.

Работа поступила в ОНТИ 3.08.90г.

Подписано в печать 8.08.90г.

Печать офсетная. Бумага для множительных аппаратов.

Формат 60x84/16. Уч.-изд. л. - 1,25. Усл. п. л. - 1,75.

Заказ No 4830. . Тираж 100 экз.

Бесплатно

Отпечатано в лаборатории офсетной печати и множительной техники Отдела научно-технической информации НИИЯФ МГУ

119899, Москва ГСП